Percolation of binary mixtures adsorbed on square lattices

F.O. Sanchez-Varretti [a], G.D. García [a], P.M. Centres [b], A.J. Ramirez-Pastor [b],*

[a] *Universidad Tecnológica Nacional, Regional San Rafael, Gral. Urquiza 314, 5600 San Rafael, Mendoza, Argentina*
[b] *Departamento de Física, Instituto de Física Aplicada, Universidad Nacional de San Luis-CONICET, Ejército de Los Andes 950, D5700HHW, San Luis, Argentina*

H I G H L I G H T S

- Percolation properties of equilibrium adsorbed phases.
- Interacting binary mixtures adsorbed on square lattices.
- A rich variety of structural orderings were observed in the adlayer.
- Percolation thresholds and percolation phase diagrams were obtained.

A R T I C L E   I N F O

A B S T R A C T

In this paper, the adsorption of interacting binary mixtures on square lattices has been studied. By using Monte Carlo simulation and finite-size scaling analysis, the connection between the surface ordered phases and the percolating properties of the adsorbed phase has been investigated. A rich phase diagram separating a percolating from a non-percolating region has been determined. The main features of the phase diagram have been discussed in terms of simple considerations related to the interactions present in the problem.

© 2015 Elsevier B.V. All rights reserved.

1. Introduction

Percolation theory [1] is a powerful tool for modeling diversity of phenomena, such as: fire propagation, fire spreading in multi-compartment structures, spreading of computer viruses, network failures, gel formation, infectious disease epidemics, granular mixture and medical research. Due to its wide applicability [2], this theory has attracted the attention of different researchers, mathematicians, physicists, programmers, engineers, physicians, etc.

The percolation theory was derived from studying the random action of fluid-like materials as they migrate through a latticework of channels. The distribution of these channels determines the probability that they will become linked together in a *great network* that allows the flow from one end of the lattice to the other. Broadbent and Hammersley [3] gave the first mathematical formulation which was able to relate the emergence of the *great network* with the minimum concentration of channels (called by the authors *percolation threshold*) by a simplified *lattice percolation model*.

Most of the studies of percolation have taken into account that the state of sites on lattice changes irreversibly from empty to filled (occupied). This scheme of filling is known as Random Sequential Adsorption (*RSA*) model [4,5]. In the framework of

---

* Corresponding author.
E-mail address: antorami@unsl.edu.ar (A.J. Ramirez-Pastor).

Nomenclature

L	Lattice side
M	Total number of lattice sites
T	Temperature
w_{xy} $(x, y = A, B)$	Nearest-neighbor interaction energy
H	Hamiltonian of the system
c_i	Occupation number of the site i ($c_i = 0$ if empty; $c_i = 1$ if occupied by A and $c_i = 2$ if occupied by B)
P	Metropolis transition probability
$\Delta H = H_f - H_i$	Difference between the Hamiltonians of the final state and initial states
k_B	Boltzmann constant
MCS	Monte Carlo step
m	Number of MCS to calculate the averages of the adsorption quantities
r	Number of samples to calculate the averages of the percolation quantities
$N_{A(B)}$	Number of adsorbed A(B) particles
N	Total number of adsorbed particles
$R_L^{R(D)}$	Probability of finding a rightward (downward) percolating cluster, formed by A and B particles
$Q_L^{R(D)}$	Probability of finding a rightward (downward) percolating cluster, formed by A particles
R_L^I	Probability of finding a cluster, formed by A and B particles, which percolates both in a rightward **and** in a downward direction
Q_L^I	Probability of finding a cluster, formed by A particles, which percolates both in a rightward **and** in a downward direction
R_L^U	Probability of finding either a rightward **or** a downward percolating cluster, formed by A and B particles
Q_L^U	Probability of finding either a rightward **or** a downward percolating cluster, formed by A particles
R_L^A	$\equiv \frac{1}{2}\left[R_L^I + R_L^U\right]$
Q_L^A	$\equiv \frac{1}{2}\left[Q_L^I + Q_L^U\right]$

Greek symbols

$\mu_{A(B)}$	Chemical potential of A(B) particles
δ's	Kronecker delta functions
ϵ_0	Interaction energy between a monomer (type A or B) and a lattice site
$\theta_{A(B)}$	Partial surface coverage corresponding to the A(B) species
θ	Total surface coverage
θ_c	Percolation threshold

adsorption, the *RSA* has been used to modeling the electro-oxidation of ethanol, characterizing the coverage and percolation properties [6], or to study deposition of proteins and colloids from solution onto solid surfaces [7].

Outside the framework of lattice and *RSA* model, the percolation concepts have been applied to study systems composed by a binary mixture of patchy colloidal particles where each species has three coupling of two types, one of which promotes bonding of particles of the same species while the other promotes bonding of different species. Then, depending on the values of the parameters of the system four distinct percolating phases can be found: two gels where only one of the species is percolated, a mixed gel where the two species are percolated but neither species percolates by itself, and a bicontinuous gel where the two species percolate independently, forming two interpenetrating spanning networks [8]. Another interesting instance, in which the percolation concepts are applied is for analyzing a mixture of liquids, Dougan et al. [9] has shown the formation of clustering structure of both species for a mixture of methanol and water as a function of concentration.

Returning to *RSA* model, the temperature does not play any relevant role and it is not considered. This model is appropriate for many physical, chemical, and biological processes where the microscopic steps are irreversible, and where equilibration is not possible on the time scale of the experiment [4]. However, in numerous systems of both theoretical and practice importance, where the adsorbed particles are in thermodynamic equilibrium, the spatial distribution of the adsorbate might be characterized by using the percolation model [10,11]. In these cases, the temperature governs the phase in the system and can be an important controlling factor in the percolation process. In this context, Giménez et al. [12,13] introduced a model in which they studied the percolation properties of the adsorbed phase of interacting monomers on a square lattice.

In this paper, the percolation behavior of an adsorbed binary mixture has been investigated by using Monte Carlo (MC) simulation and finite-size scaling analysis. For this purpose, a square substrate is exposed to an ideal *A*–*B* mixed-gas phase, at temperature T and chemical potentials μ_A and μ_B. Then, the main percolation properties of the adsorbed monolayer are obtained regarding different repulsive interactions between the adparticles.

The adsorption thermodynamics of the present model was studied in a recent paper by our group [14]. The calculations were carried out by combining theoretical modeling and MC simulations in grand canonical ensemble. Two theoretical

strategies were used: (i) the first, denoted as cluster approximation, is based on exact calculations of configurations on finite cells; and (ii) the second is a generalization of the classical quasi-chemical approximation in which the adsorbate is a binary mixture of species A and B. An exhaustive comparative analysis between theoretical and simulation results allowed us (1) to validate the MC data, and (2) to identify and characterize the most prominent features of the process of adsorption of mixtures with inter- and intra-species interactions. The present study is a natural continuation of our previous work [14] and focuses on the percolation properties of the adsorbed monolayer. The paper is organized as follows: in Section 2, the basic definitions are given along with the general basis of the MC simulation. Finally, results and conclusions are presented in Section 3.

2. Theory and simulations

The adsorption process is usually analyzed in isothermal experiments where the adsorption isotherm provides the relevant information [15]. For a mixture of two gases, the adsorbed phase will be composed of particles from both of them and the arising surface structures (if any) may be studied as the pattern/s resulting from the positions of the particles of a single or both components.

On the other hand, the central idea of the percolation problem is based on finding the minimum concentration for which a cluster extends from one side to the opposite one of the system. The percolation cluster may arise from either one component independently, or as a consequence of the mixture of particles [8].

2.1. Adsorption

The model considered here is a particular case of the Blume–Emery–Griffiths model [16], which is a very general model, used in a variety of phenomena from liquid helium phase separation to phase transitions in adsorbed films.

The adsorptive surface is represented by a two-dimensional square lattice of $M = L \times L$ adsorption sites, with periodic boundary conditions. The substrate is exposed, at a temperature T, to an ideal gas phase consisting of a binary mixture of A and B particles with chemical potentials μ_A and μ_B, respectively. Particles can be adsorbed on the lattice with the restriction of, at most, one particle per site and we consider a nearest-neighbor (NN) interaction energy w_{xy} ($x, y = A, B$) between them. The adsorbed phase is then characterized by the Hamiltonian:

$$H = \frac{1}{2} \sum_i^M \left\{ \sum_{l \in \{NN,j\}} \left[w_{AA}\delta_{c_i,c_l}\delta_{c_i,1} + w_{BB}\delta_{c_i,c_l}\delta_{c_i,2} + w_{AB}\left(\delta_{c_i,1}\delta_{c_l,2} + \delta_{c_i,2}\delta_{c_l,1}\right) \right] \right.$$
$$\left. + \epsilon_0 \sum_i^M \left(\delta_{c_i,1} + \delta_{c_i,2}\right) - \sum_i^M \left(\mu_A\delta_{c_i,1} + \mu_B\delta_{c_i,2}\right) \right\} \tag{1}$$

where c_i is the occupation number of the site i ($c_i = 0$ if empty; $c_i = 1$ if occupied by A and $c_i = 2$ if occupied by B); $l \in \{NN, j\}$ runs on the four NN sites of the site i; the δ's are Kronecker delta functions and ϵ_0 is the interaction energy between a monomer (type A or B) and a lattice site. In this contribution, the chemical potential of one of the components is fixed throughout the process ($\mu_B = 0$), while the other one (μ_A) is variable, as it is usually assumed in studies of adsorption of gas mixtures [17–21]. In the actual implementation of the model ϵ_0 was set equal to zero, without loss of any generality.

The adsorption process is simulated through a grand canonical ensemble MC method. For a given value of the temperature T and chemical potentials μ_A and μ_B, an initial configuration of A and B particles adsorbed at random positions is generated. Then an adsorption–desorption process is started, where a site is chosen at random and an attempt is made to change its occupancy state with probability given by the Metropolis rule [22]

$$P = \min\{1, \exp(-\Delta H/k_B T)\}, \tag{2}$$

where $\Delta H = H_f - H_i$ is the difference between the Hamiltonians of the final state and initial states and k_B is the Boltzmann constant. A MC step (MCS) is achieved when M sites have been tested to change its occupancy state (interested readers are referred to Ref. [20] for a more complete description of the algorithm to carry out an elementary MCS). The approximation to thermodynamical equilibrium is monitored through the fluctuations in the number of the adsorbed particles; this is usually reached in 10^6 MCS. For high values of $w_{xy}/k_B T$ up to 10^8 MCS had to be used because fluctuations are greatly enhanced. After that, the total and partial isotherms are obtained as simple average over m successive configurations:

$$\theta(\mu_A, \mu_B) = \frac{\langle N \rangle}{M}, \qquad \theta_A(\mu_A, \mu_B) = \frac{\langle N_A \rangle}{M}, \qquad \theta_B(\mu_A, \mu_B) = \frac{\langle N_B \rangle}{M}, \tag{3}$$

where $N_{(x,y)}$ is the number of adsorbed particles for species (x, y), $N = N_A + N_B$ and the brackets mean time average over the $m = 10^6$ MC simulations runs.
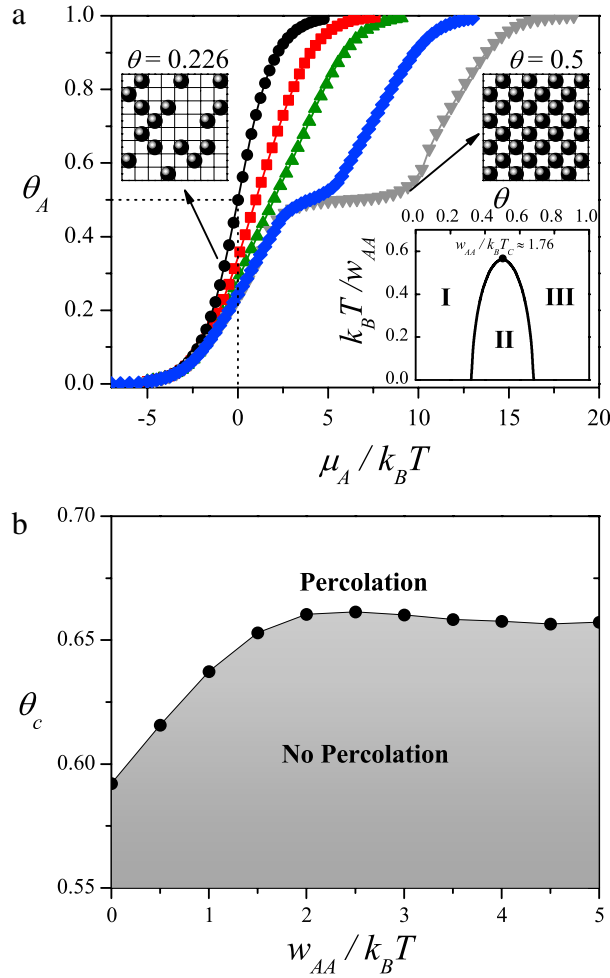
Fig. 1. (a) Adsorption isotherms for the single-gas adsorption of *A* particles onto a homogeneous surface showing the effect of lateral AA interactions: circles, $w_{AA}/k_BT = 0$; squares, $w_{AA}/k_BT = 1$; up triangles, $w_{AA}/k_BT = 2$; diamonds, $w_{AA}/k_BT = 3$ and down triangles, $w_{AA}/k_BT = 4$. Right[Left]-top inset: Typical equilibrium configuration of the adlayer for $w_{AA}/k_BT = 4$ and $\theta = 0.5$ [$\theta = 0.226$]. Solid circles and empty squares represent occupied sites and vacancies, respectively. Right-bottom inset: Temperature-coverage phase diagram corresponding to a lattice–gas of repulsive monomers ($w_{AA}/k_BT > 0$) adsorbed on a homogeneous square lattice. (b) Percolation phase diagram, which shows the curve separating the percolating and non-percolating regions for the data of part (a).

2.2. Percolation

To understand the percolation transition, we shall describe the stages of the percolation process on a lattice of sites which are occupied with probability θ or empty (non-occupied) with probability $(1 - \theta)$. Nearest-neighboring occupied sites form structures called clusters. Quantities relevant to percolation will depend on the concentration of sites and geometry of the lattice.

When the concentration is low, sites are either isolated or in small clusters of adjacent elements. As θ increases, the average size of the clusters increases monotonically. When the occupation probability exceeds a critical value (the percolation threshold θ_c), a macroscopic, lattice spanning, or an infinite cluster, occupying a finite fraction of the total number of sites, emerges. The *percolation threshold* is the concentration of sites for which, in an infinite system, a large cluster, spanning from one side to the opposite of the lattice, emerges. The percolation transition is a geometrical phase transition where the critical concentration separates a phase of finite clusters ($\theta < \theta_c$) from a phase where an infinite cluster is present ($\theta > \theta_c$). This transition is a second-order phase transition and can be characterized by well-defined critical exponents.

It is well known that it is a quite difficult matter to analytically determine the value of the percolation threshold for a given lattice [1]. Thus, in most cases, percolation thresholds have to be estimated numerically by means of computer simulations.

As the scaling theory predicts [23–26], the larger the system size to study, the more accurate the values of the threshold obtained therefrom. Thus, the finite-size scaling theory give us the basis to achieve the percolation threshold and the critical exponents of a system with a reasonable accuracy. For this purpose, the probability $R = R_L^X(\theta)$ [$Q = Q_L^X(\theta)$] of finding
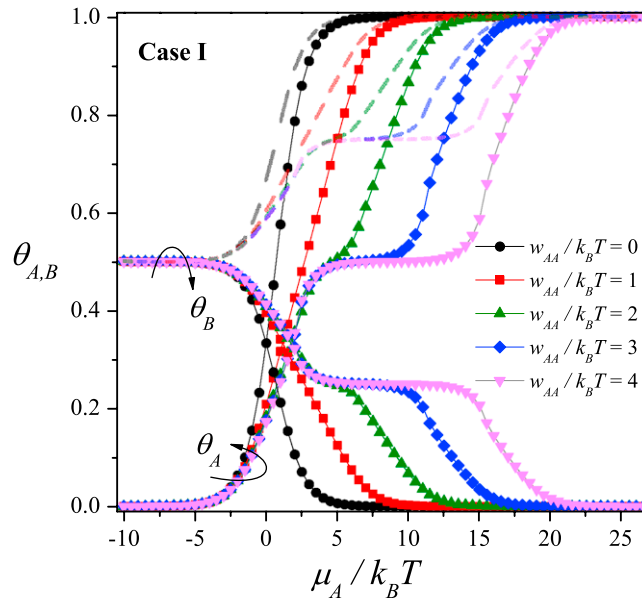
Fig. 2. Mixed-gas adsorption on a square lattice for case I. The adsorption isotherms for *A* and *B* particles (symbols) and total isotherms (dashes lines) are shown.

a percolating cluster, formed by *A* and *B* particles [formed by *A* particles], on a lattice of side *L* at concentration θ can be defined [1]. Here, the following definitions can be given according to the meaning of *X*: (a) $R_L^{R(D)}(\theta)[Q_L^{Q(D)}(\theta)]$ = the probability of finding a rightward (downward) percolating cluster; (b) $R_L^I(\theta)[Q_L^I(\theta)]$ = the probability of finding a cluster which percolates both in a rightward **and** in a downward direction; (c) $R_L^U(\theta) = [Q_L^U(\theta)]$ the probability of finding either a rightward **or** a downward percolating cluster and (d) $R_L^A(\theta) \equiv \frac{1}{2}\left[R_L^I(\theta) + R_L^U(\theta)\right]$ $\{Q_L^A(\theta) \equiv \frac{1}{2}\left[Q_L^I(\theta) + Q_L^U(\theta)\right]\}$.

In the MC simulations, $R = R_L^X(\theta)$ $[Q = Q_L^X(\theta)]$ is determined according to the following procedure:

(1) Set the value of μ_A/k_BT, μ_B/k_BT, w_{AA}/k_BT, w_{BB}/k_BT and w_{AB}/k_BT.
(2) Apply the dynamic described in Section 2.1 until the system reaches equilibrium (typically $10^6 - 10^8$ MCS).
(3) Generate $r = 10^4$ samples in equilibrium.[1] To avoid spurious correlations, the spacing between samples is set to 1000 MCS.
(4) Once the set of *r* is obtained, calculate $\theta, \theta_A, \theta_B, R_L^I(\theta), R_L^U(\theta), R_L^A(\theta), Q_L^I(\theta), Q_L^U(\theta)$ and $Q_L^A(\theta)$ as simple averages. In the case of the probabilities *R* and *Q*, the Hoshen and Kopelman algorithm [27] is used to determine the number of percolating samples.

For each obtained value of θ, the procedure 1–4 is repeated for different lattice sizes, *L* (*L* = 16, 32, 64, 128).

The standard theory of finite-size scaling [1,23,26] allows for various efficient routes to estimate θ_c from MC data. One of these methods is from the crossover of the different curves of R^X (Q^X), corresponding to distinct system sizes. Curves of R^X (Q^X) cross each other in a unique universal point, R^{X*} (Q^{X*}), which depends on the criterion *X* used. The abscissa of this point is the percolation threshold θ_c [26].

Another alternative way to estimate θ_c is from the extrapolation of the positions $\theta_c^X(L)$ of the maxima of the slopes of $R_L^X(\theta)$ $[Q_L^X(\theta)]$. For each criterion one expects that [1],

$$\theta_c^X(L) = \theta_c^X(\infty) + A^X L^{-1/\nu} \tag{4}$$

where A^X is a non-universal constant. The maximum of the differences between $|\theta_c^U(\infty) - \theta_c^A(\infty)|$ and $|\theta_c^I(\infty) - \theta_c^A(\infty)|$ gives the error bar for each determination of $\theta_c(\infty)$.

3. Results and conclusions

We focus on the case of repulsive lateral interactions, $w_{AA}/k_BT \geq 0$, $w_{BB}/k_BT \geq 0$ and/or $w_{AB}/k_BT \geq 0$, where a rich variety of structural orderings are observed in the adlayer.

---

[1] As is well known, the relaxation time increases very quickly as the ratio w_{xy}/k_BT increases. Consequently, MC simulations for strongly interacting adsorbates are very time-consuming and may produce artifacts related to non-accurate equilibrium states. To discard this possibility, equilibration times of the order of 10^8 MCS were used for values of w_{xy}/k_BT higher than 1.5. Under these conditions, the finite-size scaling study was carried out for lattice sizes of up to *L* = 128, with an effort reaching almost the limits of our computational capabilities.
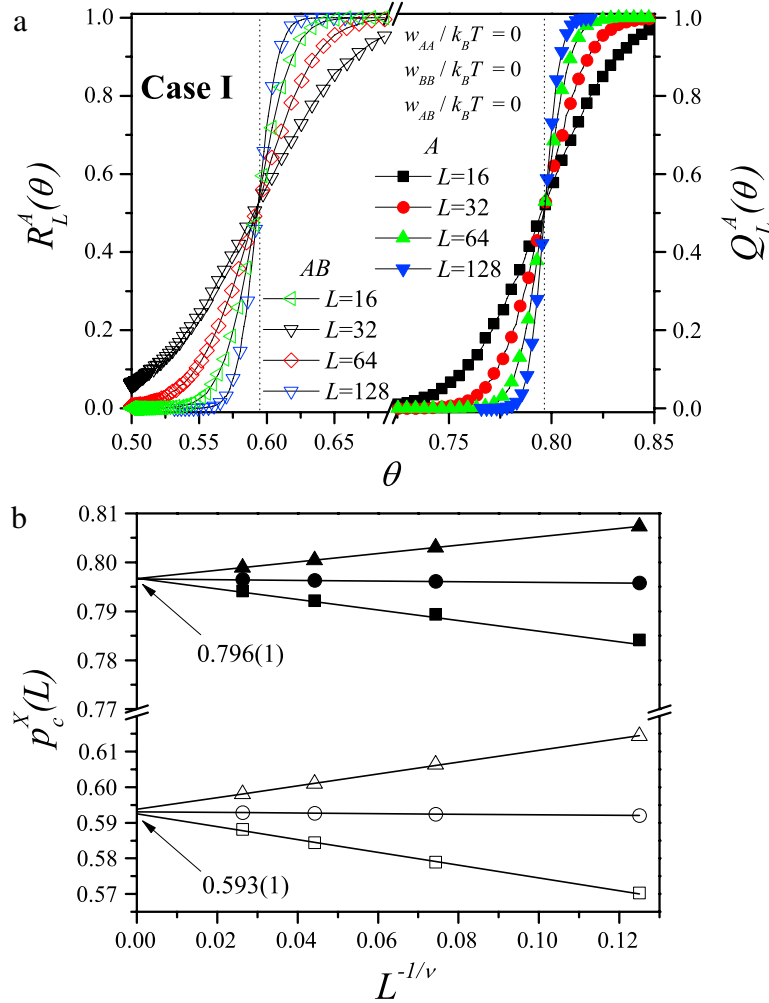
Fig. 3. (a) The percolation probability as a function of the total coverage $\theta = \theta_A + \theta_B$ for non-interacting mixtures of monomers (case I with $w_{AA}/k_BT = 0$) and different lattice sizes as indicated. Solid and open symbols correspond to A and AB percolation, respectively. In each case, the crossing of the curves indicates the percolation threshold. (b) Extrapolation of $\theta_c^X(L)$ towards the thermodynamic limit (Eq. (4)) for the cases reported in part (a). Squares, triangles and circles denote the values of $\theta_c^X(L)$ obtained by using the criteria I, A and U, respectively.

In order to understand the basic phenomenology, we analyze in the first place (Fig. 1(a)) the behavior of the adsorption isotherms for a single species, different interaction strengths and $L = 128$. For this purpose, we can consider one of the two species, A or B, with $\mu_{A(B)}/k_BT \rightarrow -\infty$, thus we have the adsorption problem corresponding to species $B(A)$.

As expected, the well-known Langmuir isotherm [28], passing through the point ($\mu_A/k_BT = 0, \theta_A = 1/2$) is obtained for $w_{AA}/k_BT = 0$. The top insets in Fig. 1(a) show two different configurations of the adlayer. In the left-top inset we can see the resulting surface formed by adsorbed particles as the repulsive interaction between A particles is increased, at zero chemical potential and coverage asymptotically approaching $\theta \approx 0.226$. In the right-top inset we can see the $c(2 \times 2)$ ordered surface structure; this phase appears when the interaction between A particles is more than a critical value $w_c/k_BT \approx 1.76$ (value of the reduced critical temperature for the order–disorder phase transition occurring in the system) [29].

The complete temperature-coverage phase diagram of the system is shown in the right-bottom inset of Fig. 1(a). Regions I, II and III correspond to a "vacancy-rich" disordered state, an ordered state [$c(2 \times 2)$ phase], and a "vacancy-poor" disordered state, respectively [29].

In Fig. 1(b), the percolation phase diagram resulting from the isotherms in Fig. 1(a) is shown. The critical curve begins at $\theta_c = 0.592$, for $w_{AA}/k_BT = 0$. In this point, the system is fully equivalent to the random percolation problem. As w_{AA}/k_BT is increased, two regimes can be distinguished: (1) From $w_{AA}/k_BT = 0$ up to $w_{AA}/k_BT \approx 1.76$, θ_c increases linearly with w_{AA}/k_BT. Repulsive couplings do not favor the nucleation, and consequently, increase the percolation threshold. This stage finishes when w_{AA}/k_BT reaches the critical value. (2) For $w_{AA}/k_BT > 1.76$, θ_c remains almost constant as w_{AA}/k_BT is increased. We say "almost", because a slight decrease is observed in the curve separating the percolating and non-percolating regions for $w_{AA}/k_BT > 3.0$. This behavior is associated with a change in the structure of the adlayer, which passes from
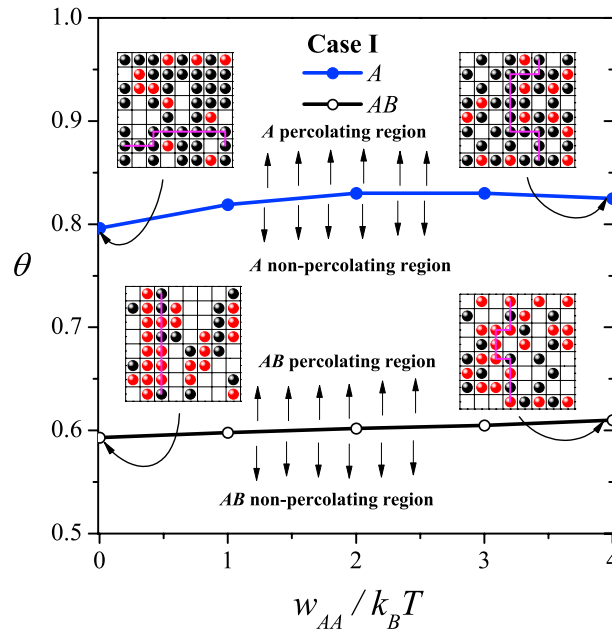
Fig. 4. Temperature-coverage phase diagram for case I: lines with solid circles, *A* percolation; and lines with open circles, *AB* percolation. The different phases are shown schematically in the insets. Black circles, red circles and empty squares represent *A* particles, *B* particles and vacancies, respectively. (For interpretation of the references to color in this figure legend, the reader is referred to the web version of this article.)
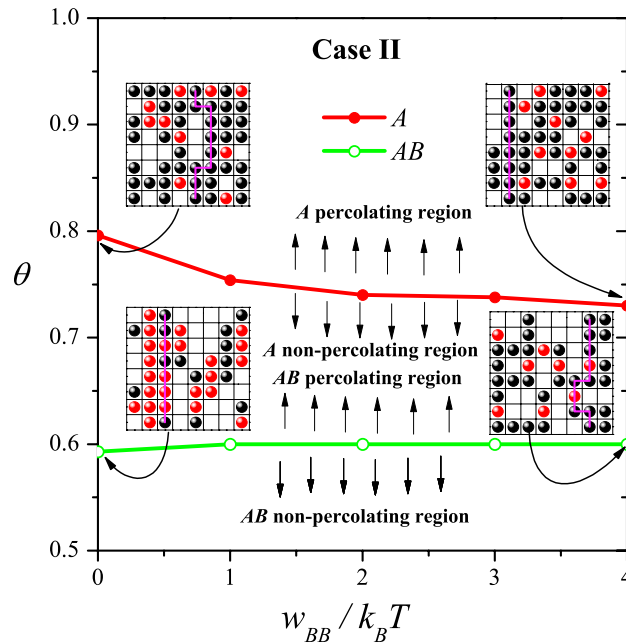

Fig. 5. Same as Fig. 4 for case II. (For interpretation of the references to color in this figure legend, the reader is referred to the web version of this article.)

region III for $\theta \approx 0.65$ and $w_{AA}/k_BT < 3.0$ to region II (close to the critical curve) for $\theta \approx 0.65$ and $w_{AA}/k_BT > 3.0$ (see right-bottom inset in Fig. 1(a)).

We will now analyze the mixture problem. In order to simplify the study of the whole phase space, which includes a wide range of values of w_{AA}/k_BT, w_{BB}/k_BT and w_{AB}/k_BT, the analysis will be divided into three cases:

case I: $w_{AA}/k_BT \geq 0$, $w_{AB}/k_BT = 0$ and $w_{BB}/k_BT = 0$;

case II: $w_{BB}/k_BT \geq 0$, $w_{AA}/k_BT = 0$ and $w_{AB}/k_BT = 0$; and

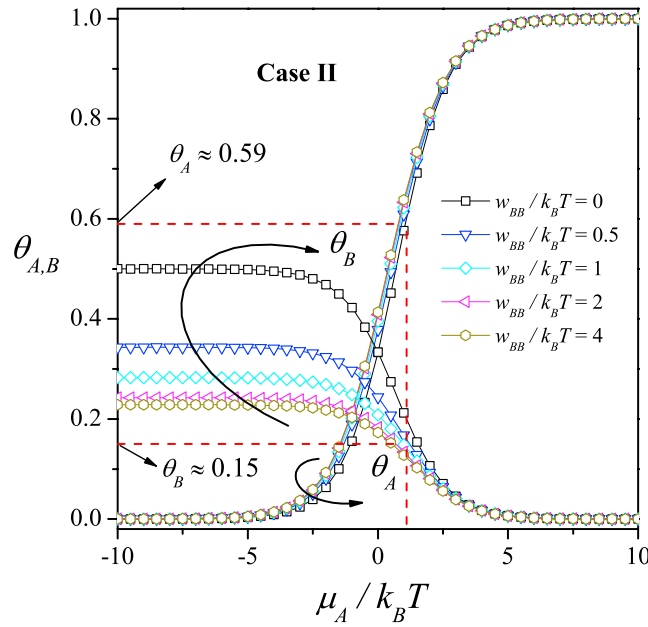*case* III: $w_{AB}/k_BT \geq 0$, $w_{AA}/k_BT = 0$ and $w_{BB}/k_BT = 0$.

Fig. 6. Mixed-gas adsorption for case II: $w_{AA}/k_BT = w_{AB}/k_BT = 0$ and different values of w_{BB}/k_BT as indicated.
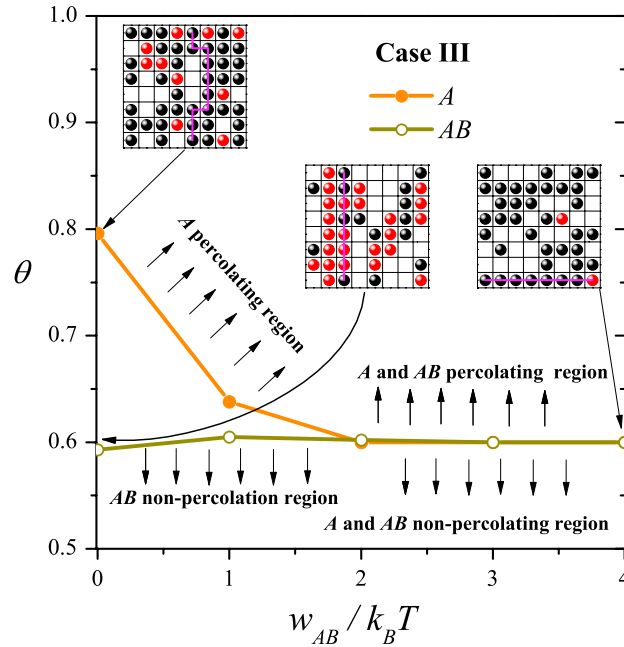

Fig. 7. Same as Fig. 4 for case III. (For interpretation of the references to color in this figure legend, the reader is referred to the web version of this article.)

A similar scheme was used in Ref. [21] to depict the configurational structures that arise in the adsorbed phase. The cases where two or more interactions are non-zero can be understood as a combination of the three cases described in the paragraph above.

For **case I**, total (dashed lines) and partial (lines and symbols) adsorption isotherms are shown in Fig. 2. The lattice size is $L = 128$. As $\mu_A \rightarrow -\infty$ the state of the system is the following: $\theta_A = 0$ and θ_B is the equilibrium coverage given by the Langmuir isotherm, $\theta_B = \exp(\mu_B/k_BT)/[1 + \exp(\mu_A/k_BT) + \exp(\mu_B/k_BT)]$, being $\theta_B = 1/2$ for $\mu_B = 0$. As μ_A is increased, the A particles adsorb on the surface and the B particles reach its equilibrium coverage in the rest of the lattice. This results in a decreasing (increasing) of the $B(A)$ isotherm.

As the interaction w_{AA}/k_BT increases, a continuous order–disorder phase transition occurs in the adlayer (plateau region) [21] and one well-defined and pronounced step appears in the partial isotherms when the interaction w_{AA}/k_BT is greater
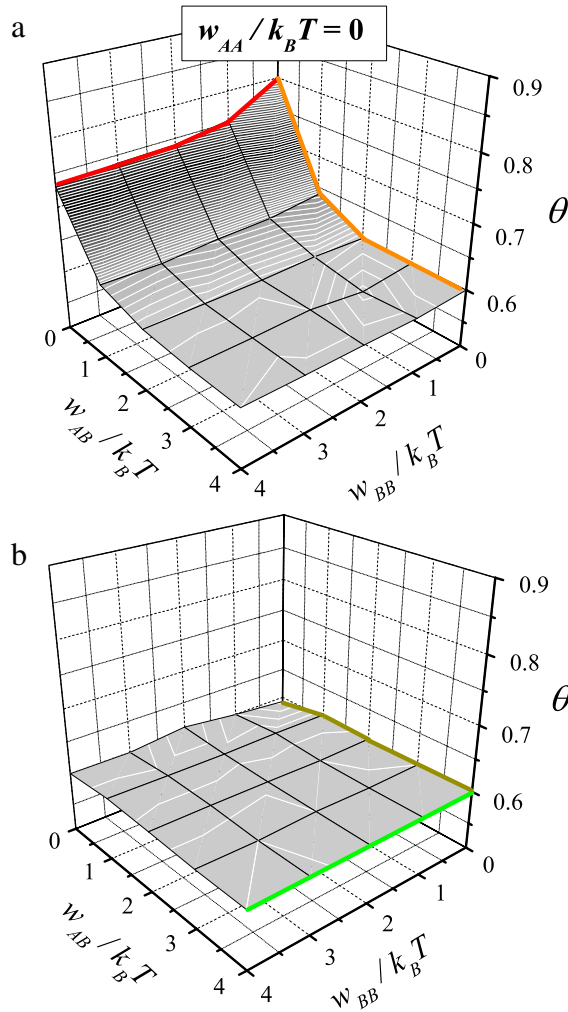
Fig. 8. Percolation phase diagram corresponding to *A* (part (a)) and *AB* (part (b)) particles for $w_{AA}/k_BT = 0$, $w_{AB}/k_BT \geq 0$ and $w_{BB}/k_BT \geq 0$. The surface in gray scale separates percolating and non-percolating regions. Limit curves represent the cases discussed in previous figures: red and green curves, Fig. 5; and orange and dark yellow curves, Fig. 7. (For interpretation of the references to color in this figure legend, the reader is referred to the web version of this article.)

than w_c/k_BT. The repulsive interaction between *A* particles determines a $c(2 \times 2)$ ordered phase and the *A* partial isotherm presents a plateau at $\theta_A = 0.5$. On the other hand, the *B* particles occupy half of the empty sites, and the corresponding *B* isotherm presents a plateau at $\theta_B = 0.25$. This behavior is a consequence of the excluded volume interaction, but it is not due to energetic interactions ($w_{BB}/k_BT = w_{AB}/k_BT = 0$ for all isotherms).

The simplest case that can be considered for a mixture of gases is when all possible energetic interactions between particles are zero. In this limit, which is analyzed in Fig. 3(a), the only interaction present is due to the excluded volume effect. The figure shows the curves of $R_L^A(\theta)$ and $Q_L^A(\theta)$ for different values of lattice size *L*. From a first inspection of Fig. 3(a) it is observed that (a) $R_L^A(\theta)$ [$Q_L^A(\theta)$] curves cross each other in a unique point; (b) those points are located at very well-defined values in the θ-axes, determining the critical percolation threshold for each case; and (c) the standard percolation problem is recovered for *AB* percolation curves giving a percolation threshold ≈ 0.59 [1].

When the percolation path is through the *A* particles, the crossing of the corresponding probability curves, $Q_L^A(\theta)$'s, shifts to $\theta_c \approx 0.795$. The origin of this effect can be understood as follows. Given that all the interactions between the adparticles are zero, the problem of percolation corresponding to the *A* particles is identical to the random percolation problem and an infinite cluster of *A* particles appears for $\theta_A \approx 0.59$. In these conditions, the *B* particles occupy 50% of the free sites left by *A* particles. Then, $\theta_B = (1 - \theta_A)/2 \approx 0.205$ and, consequently, $\theta_c = \theta_A + \theta_B \approx 0.795$.

Fig. 3(b) shows the behavior towards the thermodynamic limit of $\theta_c^X(L)$ according to Eq. (4) for the cases presented in Fig. 3(a) and $\nu = 4/3$ (random percolation). From extrapolation, one obtains $\theta_c^X(\infty)$ for the different criteria $X = U, I$ and *A*. Combining the three estimates, the final values of $\theta_c(\infty)$ can be obtained. In this case, $\theta_c^X(\infty) = 0.593(1)$ for *R* curves and
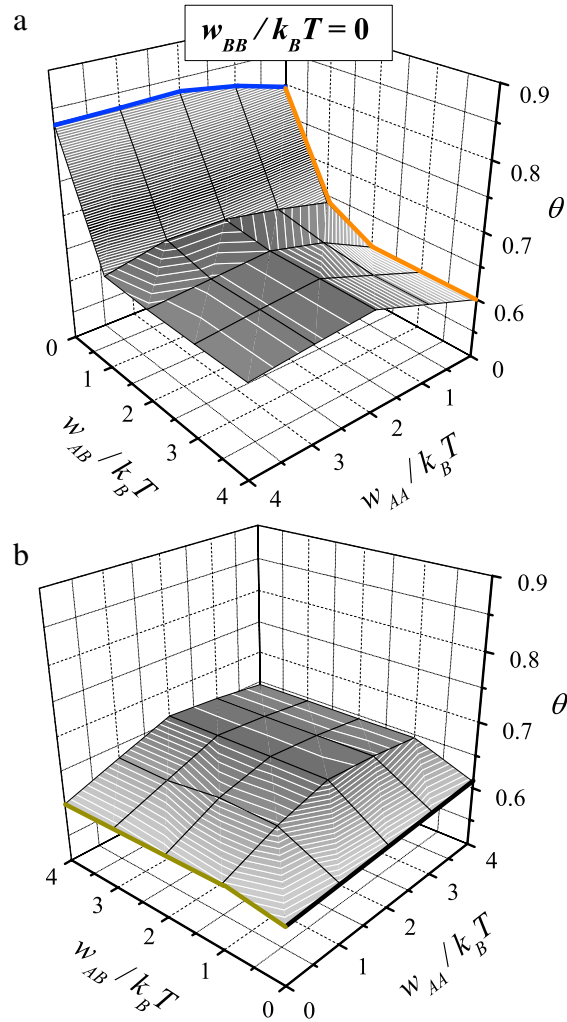
Fig. 9. Percolation phase diagram corresponding to *A* (part (a)) and *AB* (part (b)) particles for $w_{BB}/k_BT = 0$, $w_{AA}/k_BT \geq 0$ and $w_{AB}/k_BT \geq 0$. The surface in gray scale separates percolating and non-percolating regions. Limit curves represent the cases discussed in previous figures: dark and dark blue curves, Fig. 4; and orange and dark yellow curves, Fig. 7. (For interpretation of the references to color in this figure legend, the reader is referred to the web version of this article.)

$\theta_c^X(\infty) = 0.796(1)$ for *Q* curves. These values coincide, within numerical errors, with those calculated from the crossing of the curves in Fig. 3(a).

On the other hand, if the repulsive interaction between *A* particles is increased, the connectivity between nearest-neighbor sites diminishes and the percolation threshold increases, being $\theta_c \approx 0.83$ (*Q* curves) and $\theta_c \approx 0.61$ (*R* curves) for high values of w_{AA}/k_BT. Curves of $R_L^X(\theta)$ and $Q_L^X(\theta)$ are not shown here for the sake of space.

The procedure in Fig. 3 was repeated for w_{AA}/k_BT ranging between 0 and 4. The results, which are collected in Fig. 4, represent the temperature-coverage phase diagram of the system for case I. The line with solid (open) circles separates the percolating and non-percolating regions for *A* (*AB*) particle clusters. The different phases are shown schematically in the insets of Fig. 4.

In **case II**, the repulsive interaction energy between *B* particles is varied ($w_{BB}/k_BT \geq 0$) while the other interaction energies are kept at zero value ($w_{AA}/k_BT = w_{AB}/k_BT = 0$). The resulting phase diagram is shown in Fig. 5. The notation is as in Fig. 4.

When analyzing the *AB* percolation from $R_L^X(\theta)$ (curves not shown here for brevity), it is clear that the percolation threshold is $\theta_c \approx 0.59$. On the other hand, as w_{BB}/k_BT is increased, we get $\theta_c \approx 0.74$ for *A* particles (analyzed from the crossover of the $Q_L^X(\theta)$ curves). The last value can be understood from the behavior of the partial adsorption isotherms presented in Fig. 6: as previously discussed, non-interacting *A* particles require a critical concentration of the order of 0.59 to find a percolating path between two opposite sides of the system. When this situation occurs, the fraction of *B* particles on the lattice is $\theta_B \approx 0.15$ (see dotted lines in Fig. 6) and $\theta_c = \theta_A + \theta_B \approx 0.74$.
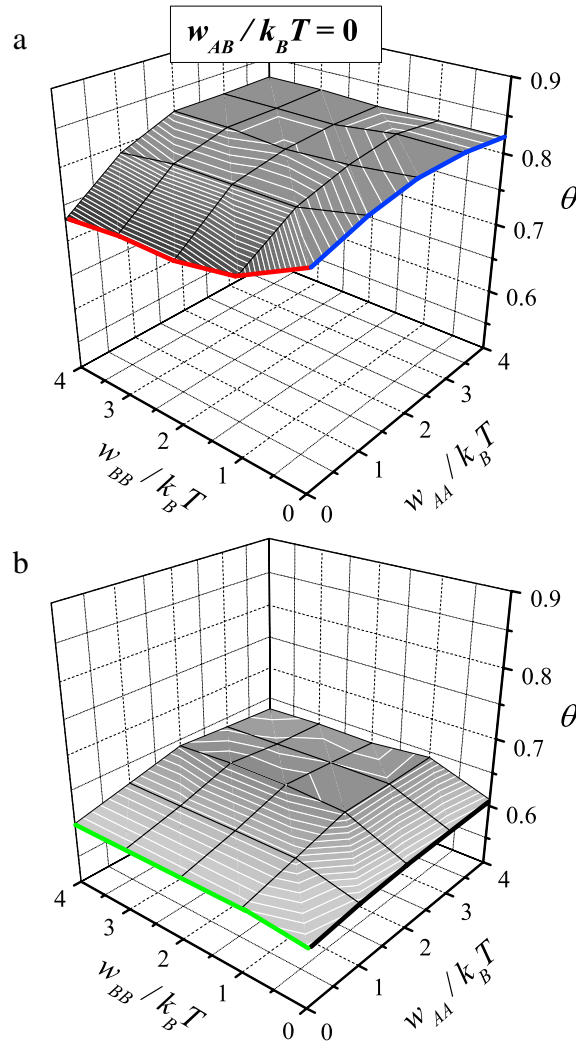
Fig. 10. Percolation phase diagram corresponding to *A* (part (a)) and *AB* (part (b)) particles for $w_{AB}/k_BT = 0$, $w_{AA}/k_BT \geq 0$ and $w_{BB}/k_BT \geq 0$. The surface in gray scale separates percolating and non-percolating regions. Limit curves represent the cases discussed in previous figures: dark and dark blue curves, Fig. 4; and red and green curves, Fig. 5. (For interpretation of the references to color in this figure legend, the reader is referred to the web version of this article.)

Case III is analyzed in Fig. 7. As it can be observed, the percolation thresholds corresponding to *A* and *AB* particles collapse in a single curve for increasing values of w_{AB}/k_BT. This behavior is due to the desorption of *B* particles produced by the adsorption of *A* particles. Namely, *B* particles desorption is enhanced by both interactions (excluded volume and energetic repulsion) between *A* and *B* particles, and the total isotherm is composed, almost exclusively, of *A* particles. Then as expected, the critical curve for *AB* particles collapses towards the *A* critical curve for $w_{AB}/k_BT > 2$.

Once we have a clear idea of the behavior of the percolation threshold for both *A* and *AB* particles with one non-zero interaction, we are ready to analyze the more complex case in which two interaction strengths are different from zero. In this context, Fig. 8 shows the case of non-interacting *A* particles. Parts (a) and (b) correspond to results obtained for *A* and *AB* percolation, respectively. In both figures, the critical surface separating the percolating and non-percolating regions is shown. A similar study is presented in Figs. 9 and 10 for $w_{BB}/k_BT = 0$ and $w_{AB}/k_BT = 0$, respectively. As described in the captions of Figs. 8–10, the highlighted curves that appear at the borders of the critical surfaces correspond to the cases discussed in Figs. 4, 5 and 7.

In summary, we presented a model to investigate the process of adsorption of a binary mixture of *A* and *B* species on a square lattice and studied the percolating properties of the adsorbed phase. We focused on the case of repulsive lateral interactions, $w_{AA}/k_BT \geq 0$, $w_{BB}/k_BT \geq 0$ and/or $w_{AB}/k_BT \geq 0$, where a rich variety of structural orderings were observed in the adlayer. By using Monte Carlo simulation and finite-size scaling theory, we obtained the percolation thresholds for different values of concentration and temperature. From this analysis, a critical curve in the $\theta - T$ space was addressed. In

each case, the line separating the percolating and non-percolating regions was explained in terms of simple considerations related to the interactions present in the problem.

Acknowledgments

References

[1] D. Stauffer, A. Aharony, Introduction to Percolation Theory, second ed., Taylor & Francis, London, 1994.
[2] M. Sahimi, Applications of Percolation Theory, Taylor & Francis, London, 1994.
[3] S.R. Broadbent, J.M. Hammersley, Proc. Cambridge Philos. Soc. 53 (1957) 629;
    J.M. Hammersley, Proc. Cambridge Philos. Soc. 53 (1957) 642.
[4] J.W. Evans, Rev. Modern Phys. 65 (1993) 1281.
[5] J. Talbot, G. Tarjus, P.R. van Tassel, P. Viot, Colloids Surf. A 65 (2000) 287.
[6] C.S. Dias, N.A.M. Araújo, A. Cadilhe, Phys. Rev. E 85 (2012) 041120.
[7] J. Feder, I. Giaever, J. Colloid Interface Sci. 78 (1980) 144.
[8] D. de las Heras, J.M. Tavares, M.M. Telo da Gama, Soft Matter 8 (2012) 1785.
[9] L. Dougan, S.P. Bates, R. Hargreaves, J.P. Fox, J. Crain, J.L. Finney, V. Réat, A.K. Soper, J. Chem. Phys. 121 (2004) 6456.
[10] Z. Gao, Z.R. Yang, Physica A 255 (1998) 242.
[11] K.Y. Gao, B.X. Liu, J. Phys.: Condens. Matter 11 (1999) 39.
[12] M.C. Giménez, F. Nieto, A.J. Ramirez-Pastor, J. Phys. A: Math. Gen. 38 (2005) 3253.
[13] M.C. Giménez, F. Nieto, A.J. Ramirez-Pastor, J. Chem. Phys. 125 (2006) 184707.
[14] F.O. Sanchez-Varretti, G.D. Garcia, P.M. Pasinetti, A.J. Ramirez-Pastor, Adsorption 20 (2014) 855.
[15] S.J. Gregg, K.S.W. Sing, Adsorption, Surface Area, and Porosity, Academic Press, New York, 1991.
[16] M. Blume, V.J. Emery, R.B. Griffiths, Phys. Rev. A 4 (1971) 1071.
[17] Y.K. Tovbin, The Theory of Physical Chemistry Processes at a Gas–Solid Interfaces, Mir Publishers & CRC Press, Boca Raton, FL, 1991.
[18] Y.K. Tovbin, in: W. Rudziński, W.A. Steele, G. Zgrablich (Eds.), Equilibria and Dynamics of Gas Adsorption on Heterogeneous Solid Surfaces, in: Studies in Surface Science and Catalysis, Elsevier, Amsterdam, 1997, p. 105.
[19] E.V. Votyakov, Y.K. Tovbin, Langmuir 13 (1997) 1079.
[20] P. Rinaldi, F. Bulnes, A.J. Ramirez-Pastor, G. Zgrablich, Surf. Sci. 602 (2008) 1783.
[21] G.D. García, F.O. Sánchez-Varretti, F. Bulnes, A.J. Ramirez-Pastor, Surf. Sci. 606 (2012) 83.
[22] N. Metropolis, A.W. Rosenbluth, M.N. Rosenbluth, A.W. Teller, E. Teller, J. Chem. Phys. 21 (1953) 1087.
[23] K. Binder, Rep. Progr. Phys. 60 (1997) 488.
[24] F. Yonezawa, S. Sakamoto, M. Hori, Phys. Rev. B 40 (1989) 636.
[25] F. Yonezawa, S. Sakamoto, M. Hori, Phys. Rev. B 40 (1989) 650.
[26] M. Dolz, F. Nieto, A.J. Ramirez-Pastor, Physica A 374 (2007) 239.
[27] J. Hoshen, R. Kopelman, Phys. Rev. B 14 (1976) 3438.
[28] I. Langmuir, J. Am. Chem. Soc. 40 (1918) 1361.
[29] J.M. Yeomans, Statistical Mechanics of Phase Transitions, Clarendon Press, Oxford, 1992.